

Creating high-purity angular-momentum-state Rydberg atoms by a pair of unipolar laser pulses

PeiPei Xin, Hong Cheng, ShanShan Zhang, HanMu Wang, ZiShan Xu, and HongPing Liu*

*State Key Laboratory of Magnetic Resonance and Atomic and Molecular Physics, Wuhan Institute of Physics and Mathematics, Chinese Academy of Sciences, Wuhan 430071, People's Republic of China
and University of Chinese Academy of Sciences, Beijing 100049, People's Republic of China*

(Received 3 January 2018; revised manuscript received 18 March 2018; published 23 April 2018)

We propose a method of producing high-purity angular-momentum-state Rydberg atoms by a pair of unipolar laser pulses. The first positive-polarity optical half-cycle pulse is used to prepare an excited-state wave packet while the second one is less intense, but with opposite polarity and time delayed, and is employed to drag back the escaping free electron and clip the shape of the bound Rydberg wave packet, selectively increasing or decreasing a fraction of the angular-momentum components. An intelligent choice of laser parameters such as phase and amplitude helps us to control the orbital-angular-momentum composition of an electron wave packet with more facility; thus, a specified angular-momentum state with high purity can be achieved. This scheme of producing high-purity angular-momentum-state Rydberg atoms has significant application in quantum-information processing.

DOI: [10.1103/PhysRevA.97.043425](https://doi.org/10.1103/PhysRevA.97.043425)**I. INTRODUCTION**

The Rydberg atom with an electronic wave packet created by an ultrafast laser is an ideal system to explore quantum dynamics and its wave-packet control has attracted considerable interest because of its great potential for application in many areas, such as quantum-information processing [1]. Recent work has shown that the Rydberg wave packets can be considered data storage registers, which have been used to successfully store and retrieve quantum information [2,3]. A typical mechanism of the Rydberg register, more precisely, is that an optical pulse carries binary information into the Rydberg atom by creating an electron wave packet (the register) where a number of states are phase flipped (binary 1) in contrast to the other states (binary 0), while another wave packet (the decoder) created by the second pulse holographically interferes with the register wave packet [4,5]. This interference process could convert the information stored as a quantum phase to amplitudes by amplifying the flipped states while other unflipped states are greatly suppressed, which has been experimentally performed [1].

Actually, the manipulation of the principal quantum number n in one coordinate of a Rydberg atom, for example, in a Stark wave packet, can be performed efficiently in a radial wave-packet database [3,6]. However, this method of information storage is limited because relatively few states couple directly to the atomic ground state via allowed transitions, and the full range of Rydberg-state quantum numbers cannot participate in quantum-information operations. Therefore, the scheme demonstrated in the above cannot be scaled to a very large and complex data register [7].

In order to facilitate more complex quantum processes, the information can be manipulated in two coordinates, for

example, in both radial and angular coordinates. Indeed, the parabolic quantum number k has been used as a second degree of freedom in quantum-information processing, which allows us to produce atomic wave packets correlated in two degrees of freedom, n and k . In addition, the angular momentum represented by the quantum number l also can be considered as the second degree of freedom for a Stark wave packet in quantum control methods [8], even though the detection of high-angular-momentum states in Rydberg atoms is difficult because they are nearly degenerate in energy. Hence, to utilize this approach for information storage, the angular-momentum content of Rydberg wave packets must be created with high purity.

To make these high-purity angular-momentum states, several works have directly utilized a quantum-mechanical approach to control the dynamic properties of Rydberg wave packets [2,5,9] while other publications have employed classical systems to manipulate the quantum system by the correspondence between classical and quantum systems in the past few years [10–12]. For instance, owing to a fast oscillating laser field, the ac Stark shift breaks the symmetry and consequently leads to angular-momentum evolution [13–15]. We can also generate nearly pure angular momentum states in Stark Rydberg wave packets by an interferometric scheme [8,16] and even manipulate the angular-momentum composition via symmetry breaking rooted in quantum defects [17].

In this paper, we propose a scheme for creating high-purity angular-momentum states utilizing a pair of unipolar optical half-cycle pulses (OHCPs) by the “tunneling-trapping” process. Eichmann *et al.* successfully exploit the n redistribution of Rydberg states with a high-polarizability laser field followed by an elliptically polarized strong laser pulse to manipulate the Rydberg atoms [18–20], where the first pulse is used to prepare an excited-state wave packet while the second one was employed to modify the shape of the bound Rydberg

*liuhongping@wipm.ac.cn

wave packet at a delayed time. Considering that the angular-momentum precession requires a shorter time scale compared to the n -selective redistribution with multicycle pulses, we find the OHCPs at the time scale of femtoseconds are able to efficiently redistribute the angular-momentum states. In addition, to rapidly operate the escaping free electron and clip the shape of the bound Rydberg wave packet in the first excitation, OHCPs in our scheme are of opposite polarity. The result shows that OHCPs are a reliable tool for creating high-purity angular-momentum-state Rydberg atoms.

II. THEORETICAL METHOD

The time-dependent Schrödinger equation (TDSE) for argon atoms in the presence of external fields can be written as [atomic units (a.u.) are used]

$$i \frac{\partial}{\partial t} \psi(\mathbf{r}; t) = [H_0 + H'] \psi(\mathbf{r}; t). \quad (1)$$

Here H_0 is the field-free Hamiltonian and H' is the laser-atom interaction. For the case of multielectron atoms, the single-active-electron (SAE) approximation, which assumes only one electron is treated explicitly while the rest of the electrons remain frozen, has been used. In the SAE approximation model, the unperturbed Hamiltonian H_0 is expressed as

$$H_0 = \frac{\mathbf{p}^2}{2} + V(\mathbf{r}), \quad (2)$$

where \mathbf{p} and \mathbf{r} are the momentum and position of the electron, respectively. In this work, we use the effective atomic potential, which is parametrized by [21]

$$V(\mathbf{r}) = -\frac{Z + a_1 e^{-a_2 r} + a_3 r e^{-a_4 r} + a_5 e^{-a_6 r}}{r}, \quad (3)$$

where Z is the charge of the residual ion and the parameters a_i are obtained by fitting the numerical potential calculated from the self-interaction free density functional theory [22].

Within the length gauge, the atom-field interaction term H' takes the form

$$H' = \mathbf{r} \cdot \mathbf{F}(t), \quad (4)$$

where $\mathbf{F}(t)$ is the time-dependent external electric field. The multicycle laser electric field $\mathbf{F}(t)$ is chosen to be of the form

$$\mathbf{F}(t) = F_0 \sin^2\left(\frac{\pi t}{\tau}\right) \cos(\omega t + \varphi) \hat{Z}, \quad (5)$$

where ω is the laser carrier frequency, φ the carrier-envelope phase (CEP), τ the total pulse duration, F_0 the peak field, and the \hat{Z} polarization direction. In the calculations of this paper, we set the CEP in Eq. (5) to zero because of its lesser impact on the population of the excited state, because in our work we used a 20-cycle pulse, which is long enough. However, for the OHCP pair, the electric field is

$$\begin{aligned} \mathbf{F}(t) = & F_{\omega_1} \sin(\omega_1 t + \varphi_1) \hat{Z} \\ & + F_{\omega_2} \sin(\omega_2(t + \Delta t) + \varphi_2) \hat{Z}, \end{aligned} \quad (6)$$

where $0 \leq t \leq \tau = T/2$ with $T = 2\pi/\omega$ the optical period. The carrier-envelope phase φ_i is used to control the parity of the unipolar field.

In the numerical calculations, $\psi(\mathbf{r}; t)$ is expanded as

$$\psi(\mathbf{r}; t) = \psi(r, \theta, \phi; t) = \sum_l \frac{R(r; t)}{r} Y_{lm}(\theta, \phi), \quad (7)$$

where the radial wave function $R(r; t)$ is expanded in the discrete variable representation (DVR) basis [23–26], and the angular part is expanded with the spherical harmonics for a fixed magnetic quantum number m . The wave-packet propagation is performed by using the split-operator method [26] to allow stable long-time evolution. Moreover, the Gauss-Lobatto quadrature is used in the DVR basis set and the expansion coefficients at the two end points are removed (set to zero) to determine where the wave function satisfies the boundary conditions. We have checked the calculation convergence for the outer boundary range (r_{\max}) and the radial grid number N . In our work, the convergent parameters for r_{\max} and N are around $r_{\max} = 1000$ and $N = 400$. In the large- r limit, we also employ an absorption potential [26] to avoid the artificial reflection of the wave packet at the boundaries.

We calculate the probability of the electron on the bound state by projecting $\psi(\mathbf{r}; t)$ onto the corresponding field-free eigenstates $\psi_{nlm}(\mathbf{r})$:

$$P_{nlm} = |\langle \psi_{nlm}(\mathbf{r}) | \psi(\mathbf{r}; t) \rangle|^2. \quad (8)$$

The probability of the electron in the quantum state n is $P_n = \sum_{lm} P_{nlm}$.

Note that in Eq. (7), there is only an $m = 0$ component if the atom is initially prepared in the s state. However, for the linearly polarized laser pulse, it is also applicable for an Ar atom in our case even though the atom is initially in the p state since the contribution of the ionization probability from $m = \pm 1$ is much smaller in comparison to the $m = 0$ component.

III. RESULTS AND DISCUSSION

In the calculation, we choose the ground electronic state ($3p$) of an Ar atom as the initial state, whose wave function is calculated by solving the eigenequation of the Ar atom in free field. With the aid of the TDSE, we can calculate the yields of Ar ions and excited neutral Ar* atoms as well. In the ionization, the tunneled electron, having escaped from the nucleus, has a certain probability to recombine with the ion core due to the Coulomb force of the ion; thus the tunneling ionization itself is dynamically suppressed, which is called frustrated tunneling ionization (FTI) [19,20,27,28]. A n population of the excited states from our calculation is checked and found to be in agreement with the experimental result by Eichmann *et al.* for He* atoms [19]. Although the neutral excited state yield is seriously dependent on the laser intensity, its n population does not change so much for laser intensity varying in a wide range [28].

Without a doubt, a pair of OHCPs can also be used to manipulate the population of the Rydberg states, providing the freedom of time delay between them for the dynamics control. For example, utilizing the laser pair visualized in Fig. 1(a), where a positive-polarity OHCP is followed by a less intense OHCP of opposite polarity (intensity ratio approximately 5:1), we can calculate the n population of the excited Rydberg states. It is shown in Fig. 1(b). We can see that the n -dependent

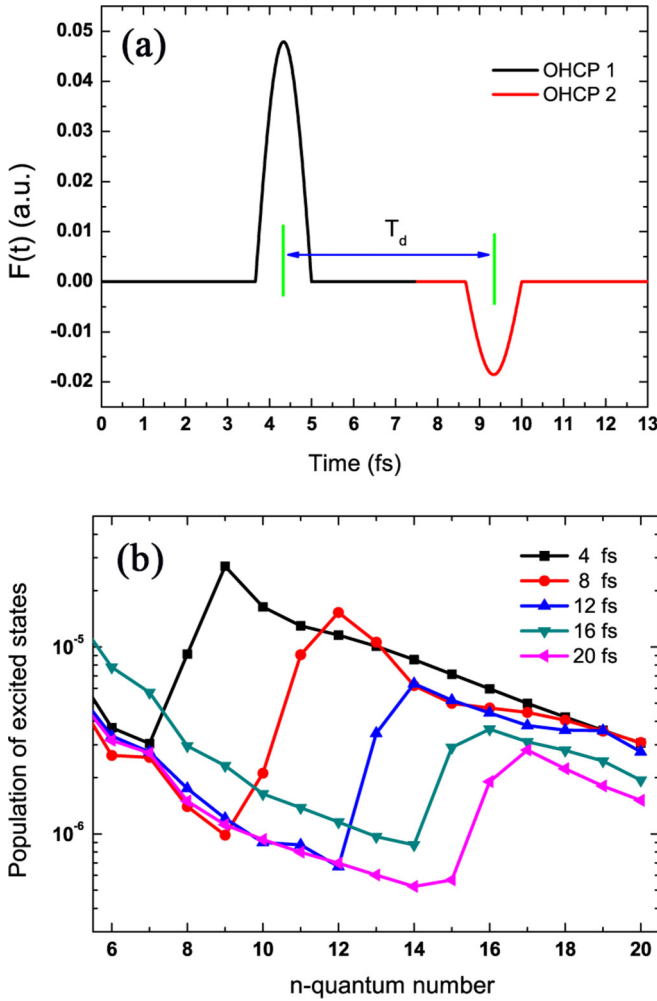


FIG. 1. The population of excited Rydberg states from TDSE calculations with a pair of OHCPs. (a) Two unipolar OHCPs are time delayed by T_d between the peak electric fields and have amplitudes with ratio approximately 5:1. (b) The n population of excited Rydberg states changes much as the time delay varying from 4 to 20 fs with two laser intensities set as 1.0×10^{14} W/cm² and 0.15×10^{14} W/cm², respectively.

neutral excited-state yield changes much as the time delay varying from 4 to 20 fs. The two laser intensities are fixed at 1.0×10^{14} and 0.15×10^{14} W/cm², respectively [29]. The whole process can be understood by a tunneling-trapping scenario, where pulse 1 serves as a “pump” field, which kicks the electron from the ground state and initiates an outgoing electron wave packet while pulse 2 traps the outgoing electron in excited states for its reverse direction to clip the shape of the outgoing electron wave packet at the appropriate time delay. This sensitive response of the n population has been well explained by an impulsive momentum kick model and energy conservation law in the free propagation process [30–35]. When the time delay between two pulses is set to a large value, the electron has more probability to escape away from the nucleus to a larger distance r_t and the tunneling electron owns only a small momentum p_t , which makes it undergo a weaker trapping force, and higher n quantum states are thus created.

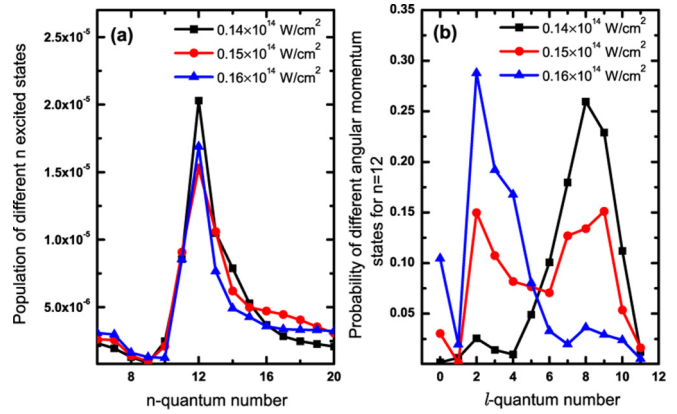


FIG. 2. (a) The n distribution of the population of excited states and (b) the corresponding probability of different angular-momentum states for the most populated quantum number ($n = 12$) as a function of the OHCP2 strength, with the strength of OHCP1 of 1.0×10^{14} W/cm² and a fixed time delay of $T_d = 8$ fs.

The OHCP pair scheme not only provides a universal way to selectively excite atoms into an appropriate n state with a proper time delay [Fig. 1(b)], but also conveniently generates specified high-purity angular-momentum states. Here the purity is defined as the ratio of the population of the single angular-momentum state to the populations of all states in the same n manifold, which has been used in many references [2,8]. It is found that an angular purity greater than 30% is enough to realize the storage and retrieval of information in a Rydberg-atom data register experimentally [2]. Once we optimize the time-delay parameter to get a specified n distribution of excited states in our scheme [for example, the most population around quantum number $n = 12$, as shown in Fig. 2(a)], we can continue to tune the parameters such as the laser intensity to investigate if it is possible to manipulate the angular-momentum distribution of the excited state. Theoretically, the second pulse, OHCP2, can affect the electron reverse dynamics and then change the angular momenta of the Rydberg state by strongly coupling different angular-momentum states via tuning its intensity. As the n population of the excited state is immune to the laser intensity, as shown in Fig. 2(a), it will be meaningful if we can manipulate the angular-momentum population of excited atoms.

Figure 2(b) shows the probability of different angular-momentum states for the most populated quantum number ($n = 12$) as a function of the OHCP2 strength at the optimized time delay, $T_d = 8$ fs. Clearly, a gradual change in the angular-momentum-state distributions is observed with increasing OHCP2 strength. For the case of lower intensity of OHCP2 in 0.14×10^{14} W/cm², the most population is dominated by the high-angular-momentum states. When the intensity of OHCP2 increases up to a high value of 0.16×10^{14} W/cm², however, the major contribution comes to the low-angular-momentum states ($l_{\max} = 2$). These two cases all have a single peak in the angular-momentum distribution. Moreover, in the case of medium intensity (0.15×10^{14} W/cm²) of OHCP2, we get a bimodal pattern of population which has the lowest distribution around $l = n/2$.

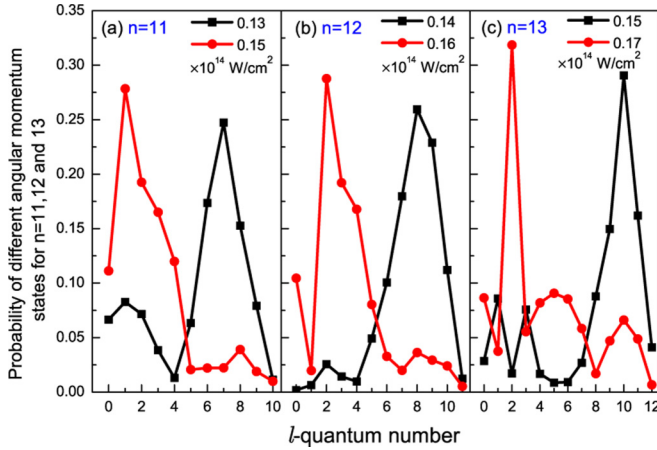


FIG. 3. The probability of angular-momentum states for different principal quantum number ($n = 11, 12, 13$) as a function of the OHCP2 strength. The laser strength of OHCP1 is the same as in Fig. 2 and the time delays between the two unipolar optical OHCPs are 6, 8, and 10 fs, respectively. The population redistribution shows very similar behavior.

This angular-momentum selective population technique also works for other chosen principal quantum numbers, which are demonstrated for $n = 11, 12$, and 13 as shown in Fig. 3. As expected, the behavior of adjoining principal quantum number is similar, which proves a general feature of this scheme. It can also be seen that utilizing these sequences of unipolar laser pulses can create the high-purity states with not only low- l but also high- l states. In previous works [2,8,9], so far, the achieved purity of low- l states such as $25p \sim 28p$ is about 30% while that for $l = 23$ or 24 in the $n = 25$ manifold is only 10%. Moreover, in our calculation, one interesting phenomenon is that the absolute population of high-purity states shows a slight increasing trend as n increases. For instance, the low- l component ($l = 1$) in the Rydberg wave packets for $n = 11$ occupies 27% of the total angular-momentum-state population but the maximum population of the $n = 13$ state can be enhanced to 32%. A similar tendency is shown for the high- l states. More interesting is that the angular-momentum-state distribution gets narrower for higher n manifold as shown in Fig. 3(c), where the $l = 2$ state for $n = 13$, for example, has a much higher purity while the other states are suppressed at a laser intensity of 0.17×10^{14} W/cm² for OHCP2. The higher angular-momentum state ($l = 10$) can also be obtained at a laser intensity of 0.15×10^{14} W/cm², which is close to a circular Rydberg-state preparation.

To explain this interesting phenomenon, we present the spatial probability distributions of an excited wave packet prepared by the OHCP1 in Fig. 4 at the moment OHCP2 is applied, which well explains the narrow filtering effect in the angular-momentum distribution shown in Fig. 3. For example, as discussed previously, we have to optimize the delay time to maximally narrow the angular distribution for a specified principle quantum number n . This optimized delay time for $n = 13$ [Fig. 4(c)] is slightly longer than that for $n = 11$ [Fig. 4(a)] and $n = 12$ [Fig. 4(b)], giving a chance for the wave packet to expand more before the OHCP2 is applied. We have a look at the region inside the solid red lines in Fig. 4, where

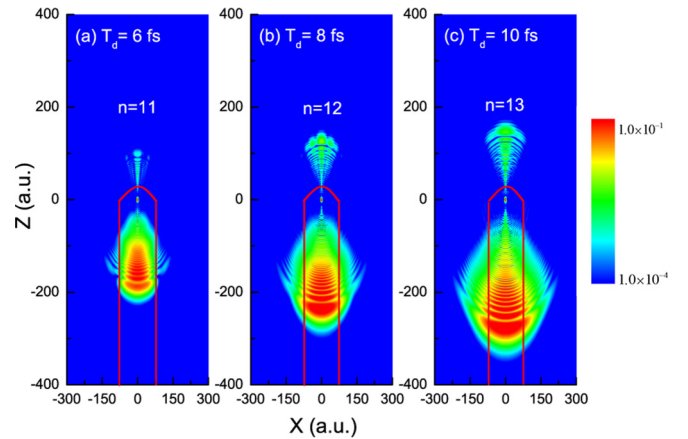


FIG. 4. Contour plots of spatial probability distributions of excited wave packet prepared by the OHCP1 in the (x, z) plane at the moment that OHCP2 acts. The electrons inside the solid red lines will be attracted towards the core and it causes different filtering effects for different wave-packet expansion. Obviously, a longer delay helps the wave packet expand more and then causes a higher resolution in filtering as shown in (c).

the electron in this area will be attracted back to the Coulomb potential after the OHCP2 is applied, but outside it the electron will be blown away, escaping from the Coulomb potential. This provides a mechanism to enhance the filtering resolution by choosing an optimized condition with longer delay time.

As shown in Figs. 2(b) and 3, we can see that the angular-momentum-state distribution is sensitively dependent on the OHCP2 strength. It is caused by the interexchange between different angular-momentum states in the wave packet driven by the laser field. This can be seen from the l -population evolution with the laser field of the applied OHCP2. It is shown in Fig. 5. When the laser intensity increases from 0.14×10^{14} to 0.15×10^{14} W/cm² [Fig. 5(a)], the angular-momentum-state population evolves from a high-angular-momentum-predominant distribution to a double-hump structure with high and low angular momentum equally weighted. After this critical point, as the laser intensity increases more, the

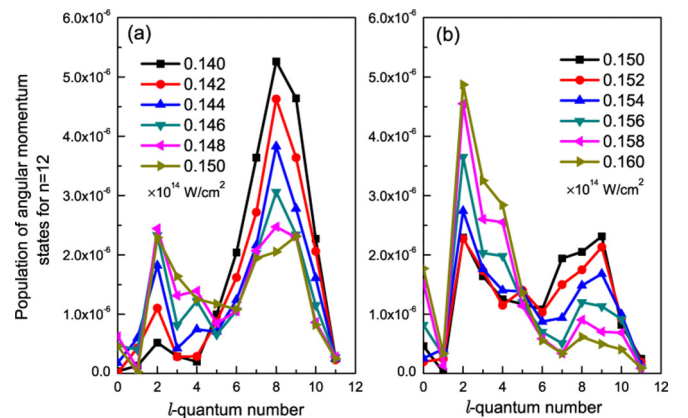


FIG. 5. The evolution of the angular-momentum-state population with increasing laser intensity of the applied OHCP2 from 0.14×10^{14} up to 0.16×10^{14} W/cm².

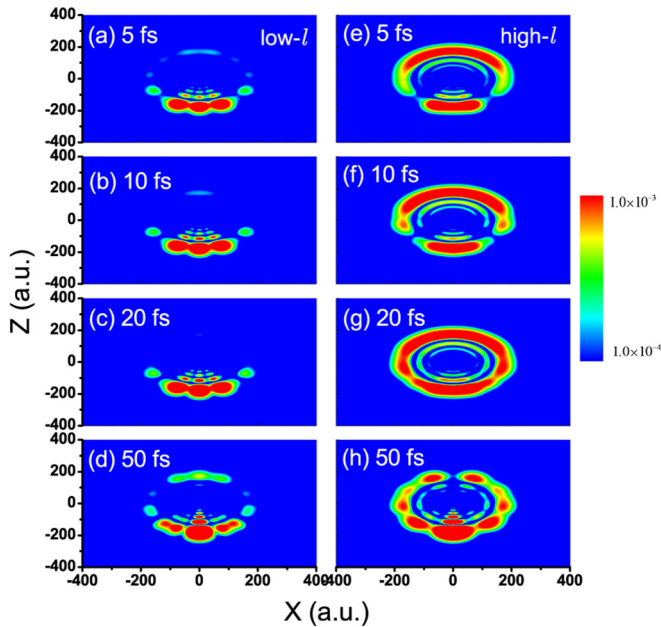


FIG. 6. Contour plots of the calculated probability wave-packet spatial distributions in the (x, z) plane of (a)–(d) low- l states and (e)–(h) high- l states at times 5, 10, 20, and 50 fs.

high-angular-momentum components continue to transfer to the low-angular-momentum parts as Fig. 5(b) and arrive at a maximum when the laser intensity goes up to 0.16×10^{14} W/cm².

It is expected that the spatial localization of the high-purity angular-momentum wave packets prepared in our method should approach the eigenwave function of the purified angular-momentum state and be time independent. It is shown in Fig. 6. It can be seen that the high-purity wave packets with low l have populated into the downhill side of the nucleus which becomes largely polar for its highly eccentric orbits. It is easily understood by the classical picture that the low- l -state electron moves very fast near the nucleus and thus spends the most time at the large- r trajectory on average. The quantum character of the low- l state is also verified by the regularly spaced nodes along r and θ as shown in Figs. 6(a)–6(d). On

the contrary, the space localization of the wave packets for the high- l states is far away from the nucleus and has a circular distribution at large r . It is shown in Figs. 6(e)–6(h).

More basically, the state-transfer process manifested in our calculation can also be understood as the rescattering of the electron whose momentum is driven by different intensities of the short laser pulse OHCP2. Essentially, our method is to tune the interference between the rescattered electron and the initial prepared wave packet, which is similar to the migration of population to specified angular-momentum Rydberg states by pulse sequencing techniques for Xe atoms [17] and the dynamics evolution of angular momentum in alkali-metal atoms [8], but in our scheme a fine adjustment of the second pulse intensity is enough. This angular-momentum manipulation scheme can be applied in quantum-information processing and can be realizable in the laboratory.

IV. CONCLUSION

In summary, we have theoretically investigated the generation of angular-momentum states with high purity in Rydberg argon atoms. Unlike the dynamic behavior of the tunneled electron only controlled by the Coulomb field in the FTI process, a regulation mechanism of Rydberg atoms based on the tunneling-trapping model had been applied in creating the angular-momentum states. Our numerical calculations indicate that the OHCP pair is a reliable tool for probing the evolution of angular-momentum states. By varying the time delay between two OHCPs and the tuning strength of OHCP2, it is possible to create high- and low-angular-momentum states with high purity, which will contribute a significant promotion for the research of Rydberg-atom quantum-information processing in a strong laser field. Moreover, this wave-packet coherent control of atomic systems will also help us to find new ways of controlling wave packets in more complex systems such as molecules.

ACKNOWLEDGMENTS

The work was supported by NSFC (Grants No. 91421305, No. 91121005, and No. 11674359) and the National Key Basic Research Program of China (Grant No. 2013CB922003).

[1] J. Ahn, T. C. Weinacht, and P. H. Bucksbaum, *Science* **287**, 463 (2000).
 [2] J. Ahn, D. N. Hutchinson, C. Rangan, and P. H. Bucksbaum, *Phys. Rev. Lett.* **86**, 1179 (2001).
 [3] C. Rangan, J. Ahn, D. N. Hutchinson, and P. H. Bucksbaum, *J. Mod. Opt.* **49**, 2339 (2002).
 [4] C. Leichtle, W. P. Schleich, I. S. Averbukh, and M. Shapiro, *Phys. Rev. Lett.* **80**, 1418 (1998).
 [5] T. C. Weinacht, J. Ahn, and P. H. Bucksbaum, *Phys. Rev. Lett.* **80**, 5508 (1998).
 [6] C. Rangan and P. H. Bucksbaum, *Phys. Rev. A* **64**, 033417 (2001).
 [7] D. A. Meyer, *Science* **289**, 1431 (2000).

[8] H. Wen, C. Rangan, and P. H. Bucksbaum, *Phys. Rev. A* **68**, 053405 (2003).
 [9] J. Ahn, C. Rangan, D. N. Hutchinson, and P. H. Bucksbaum, *Phys. Rev. A* **66**, 022312 (2002).
 [10] D. G. Arbö, C. O. Reinhold, J. Burgdörfer, A. K. Pattanayak, C. L. Stokely, W. Zhao, J. C. Lancaster, and F. B. Dunning, *Phys. Rev. A* **67**, 063401 (2003).
 [11] C. L. Stokely, F. B. Dunning, C. O. Reinhold, and A. K. Pattanayak, *Phys. Rev. A* **65**, 021405 (2002).
 [12] J. Bromage and C. R. Stroud, Jr., *Phys. Rev. Lett.* **83**, 4963 (1999).
 [13] R. Grobe, G. Leuchs, and K. Rzazewski, *Phys. Rev. A* **34**, 1188 (1986).

- [14] J. D. Corless and C. R. Stroud, Jr., *Phys. Rev. Lett.* **79**, 637 (1997).
- [15] H. M. Nilsen, J. P. Hansen, S. Selsto, and L. B. Madsen, *J. Phys. B* **32**, 4995 (1999).
- [16] C. Rangan and R. J. A. Murray, *Phys. Rev. A* **72**, 053409 (2005).
- [17] J. R. R. Verlet, V. G. Stavros, R. S. Minns, and H. H. Fielding, *Phys. Rev. Lett.* **89**, 263004 (2002).
- [18] S. Eilzer and U. Eichmann, *J. Phys. B* **47**, 204014 (2014).
- [19] T. Nubbemeyer, K. Gorling, A. Saenz, U. Eichmann, and W. Sandner, *Phys. Rev. Lett.* **101**, 233001 (2008).
- [20] U. Eichmann, T. Nubbemeyer, H. Rottke, and W. Sandner, *Nature (London)* **461**, 1261 (2009).
- [21] X. M. Tong and C. D. Lin, *J. Phys. B* **38**, 2593 (2005).
- [22] X.-M. Tong and Shih-I Chu, *Phys. Rev. A* **55**, 3406 (1997).
- [23] J. C. Light and R. B. Walker, *J. Chem. Phys.* **65**, 4272 (1976).
- [24] A. S. Dickinson and P. R. Certain, *J. Chem. Phys.* **49**, 4209 (1968).
- [25] D. O. Harris, G. G. Engerholm, and W. D. Gwinn, *J. Chem. Phys.* **43**, 1515 (1965).
- [26] X.-M. Tong and S.-I. Chu, *Chem. Phys.* **217**, 119 (1997).
- [27] U. Eichmann, A. Saenz, S. Eilzer, T. Nubbemeyer, and W. Sandner, *Phys. Rev. Lett.* **110**, 203002 (2013).
- [28] H. Zimmermann, J. Buller, S. Eilzer, and U. Eichmann, *Phys. Rev. Lett.* **114**, 123003 (2015).
- [29] B. Zhang, W. Chen, and Z. Zhao, *Phys. Rev. A* **90**, 023409 (2014).
- [30] R. R. Jones, D. You, and P. H. Bucksbaum, *Phys. Rev. Lett.* **70**, 1236 (1993).
- [31] C. O. Reinhold, M. Welles, H. Shao, and J. Burgdorfer, *J. Phys. B* **26**, L659 (1993).
- [32] A. Bugacov, B. Piraux, M. Pont, and R. Shakeshaft, *Phys. Rev. A* **51**, 1490 (1995).
- [33] F. Robicheaux, *Phys. Rev. A* **56**, R3358 (1997).
- [34] I. Bersons and A. Kulsh, *Phys. Rev. A* **59**, 1399 (1999).
- [35] A. Wetzels, A. Gürtler, L. D. Noordam, F. Robicheaux, C. Dinu, H. G. Muller, M. J. J. Vrakking, and W. J. van der Zande, *Phys. Rev. Lett.* **89**, 273003 (2002).